Acta Cryst E
CRYSTALLOGRAPHIC COMMUNICATIONS
ISSN 2056-9890

Crystal packing analysis of *in situ* cryocrystallized 2,2,2-trifluoroacetophenone

Dhananjay Dey, Abhishek Sirohiwal‡ and Deepak Chopra*

Crystallography and Crystal Chemistry Laboratory, Department of Chemistry, Indian Institute of Science Education and Research Bhopal, Bhopal 462066, Madhya Pradesh, India. *Correspondence e-mail: dchopra@iiserb.ac.in

Received 27 October 2017
Accepted 17 November 2017

Edited by C. Massera, Università di Parma, Italy

‡ Currently at Max Planck Institute for Chemical Energy Conversion, Stiftstrasse 34-36, 45470 Mülheim an der Ruhr, Germany.

Keywords: crystal structure; *in situ* cryocrystallization; fluorine-based interactions; intermolecular interaction energies; Hirshfeld surface analysis.

CCDC reference: 1578858

Supporting information: this article has supporting information at journals.iucr.org/e

Crystals of the liquid compound 2,2,2-trifluoroacetophenone (TFAP, $C_8H_5F_3O$) were obtained using the state-of-art *in situ* cryocrystallization technique. TFAP crystallizes in the monoclinic space group *C*2/*c*, and its crystal structure is mainly stabilized by a set of C—H···F, C—H···O, F···F and F···O supramolecular contacts. The overall molecular arrangement shows the formation of molecular sheets parallel to the *bc* plane, which are in turn stacked along the *a*-axis direction. The weak interactions have been studied thoroughly, performing both a Hirshfeld surface analysis and theoretical calculations, to obtain the intermolecular interaction energies. A structural comparison of this compound with the previously reported substituted analogs was also carried out, showing a qualitative difference in terms of packing behaviour.

1. Chemical context

The use of green, efficient, metal-free and inexpensive catalysts is the desire of every synthetic laboratory. The importance of metal-free catalysts is well known among synthetic chemists. In this class of catalysts, 2,2,2-trifluoroacetophenone (TFAP) is well known, because it is cheap and commercially available.

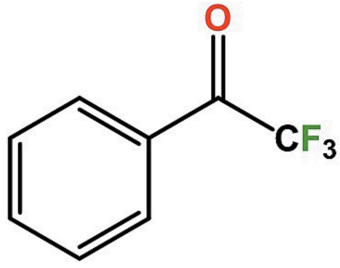

Research work in recent years has shown that TFAP can be used as a green organocatalyst in synthetic procedures, *e.g.* for the epoxidation of alkenes (Limnios & Kokotos, 2014*a*), the oxidation of allyloximes to form isoxazoline (Triandafillidi & Kokotos, 2017), the oxidation of aliphatic tertiary amines and azines (Limnios & Kokotos, 2014*b*) and for the synthesis of substituted tetra-hydrofurans (Theodorou & Kokotos, 2017*a*), indolines and pyrrolidines (Theodorou & Kokotos, 2017*b*), besides being used for the synthesis of fluorinated polymers (Guzmán-Gutiérrez *et al.*, 2008). Interestingly, TFAP has been also used for probing intermolecular interactions involved in the bi-molecular complexes formed on Pt(111) surfaces (Goubert *et al.*, 2011). In fact, TFAP is also an excellent example to study the enantioselective hydrogenation on Pt

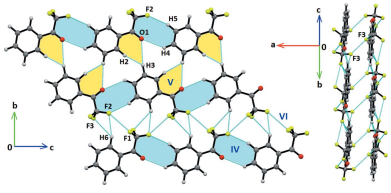

Table 1
Hydrogen-bond geometry (Å, °).

D—H···A	D—H	H···A	D···A	D—H···A
C6—H6···F1	0.95	2.48	3.004 (2)	115
C6—H6···F3	0.95	2.55	3.088 (2)	116
C5—H5···F2^{i}	0.95	2.63	3.522 (2)	156
C4—H4···O1^{i}	0.95	2.74	3.490 (2)	136
C6—H6···F2^{ii}	0.95	2.69	3.614 (2)	163
C6—H6···F3^{ii}	0.95	2.94	3.584 (2)	126
C5—H5···F3^{ii}	0.95	2.98	3.603 (2)	124
C3—H3···O1^{iii}	0.95	2.95	3.882 (2)	166

Symmetry codes: (i) $x, y, z-1$; (ii) $x, -y+1, z-\frac{1}{2}$; (iii) $x, -y, z-\frac{1}{2}$.

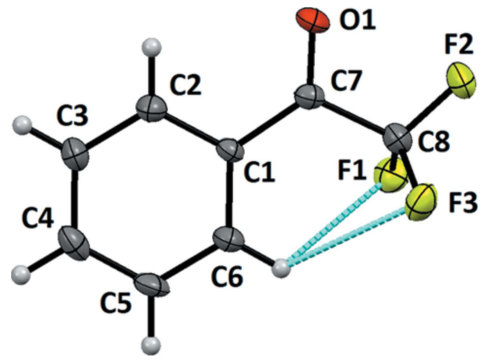

Figure 1
Displacement ellipsoid plot of TFAP drawn at the 50% probability level. Weak intramolecular interactions are shown as cyan dotted lines.

surfaces (Cakl *et al.*, 2011). Keeping in mind both the important applications of this molecule and our work on intermolecular interactions involving organic fluorine, we decided to determine the crystal structure of this compound. It is worth noting that since TFAP is a liquid at room temperature, a crystal structure determination using conventional methods is not feasible; hence, this class of compounds needs special experimental settings. The method for obtaining crystals of these compounds is called the *in situ* cryocrystallization technique (Boese *et al.*, 2003; Choudhury *et al.*, 2005). In the recent past, we have employed this technique to obtain crystal structures of both organic (Dey *et al.*, 2016*a*,*b*) and organometallic liquids (Sirohiwal *et al.*, 2017*a*). We believe that this study delineates the importance of fluorine-based interactions, in addition to other weak interactions, which play a role in the crystal packing of TFAP.

2. Computational methodology

All the calculations were performed at the crystal geometry, where hydrogen-atom positions are fixed to their respective neutron values (Allen, 1986). The lattice and intermolecular interaction energies were computed using the PIXELC module of the *CLP* program (Version 12.5.2014; Gavezzotti, 2003, 2011), which partitions the total energy into Coulombic, polarization, dispersion and repulsion energies. For the same purpose, the molecular electron density was computed at the MP2/6-31G (d, p) level of theory using *Gaussian09* (Frisch *et al.*, 2009).

3. Structural commentary and supramolecular features

The single-crystal X-ray diffraction analysis reveals that the title compound crystallizes in the space group *C*2/*c*, and confirms the presence of one –$COCF_3$ functional group attached to the phenyl ring (see Fig. 1). The backbone of the molecule formed by the atoms O1/C1–C8 is essentially planar, with a maximum deviation from the plane of 0.053 (1) Å for C8. In the molecule, two intramolecular C—H···F interactions are present, involving C6—H6 and the atoms F1 and F3 (C6—H6···F1, 2.48 Å and 115°; C6—H6···F3, 2.55 Å and 116°; Table 1). A total of seven molecular pairs are extracted from the crystal packing based on their stabilizing contribution towards the total lattice energy. Their detailed energy decomposition analysis is listed in Table 2. These molecular pairs are associated through various intermolecular interactions involving aromatic C—H groups as donors and C—F and C═O moieties as acceptors. The crystal packing is further

Table 2
Stabilization energies (in kJ mol^{-1}) of the individual molecular pairs.

CD = centroid–centroid distance.

Motif	Symmetry	CD (Å)	E_{Coul}	E_{Pol}	E_{Disp}	E_{Rep}	E_{Tot}	Possible Interactions	Geometry (Å, °)
I	$-x+1, y, -z+\frac{3}{2}$	3.731	−5.6	−1.7	−26.2	14.6	−18.8	C7···C6	3.6668 (1)
								C1···C1	3.6035 (1)
								C2···C2	3.5545 (1)
								C8—F3···F3—C8	2.8743 (1), 139, 139
II	$-x+\frac{1}{2}, -y+\frac{1}{2}, -z+1$	5.470	−3.5	−0.9	−20.4	10.2	−14.5	π–π stacking	3.7869 (1)
								C8—F1···C4	3.2425 (1), 134
III	$-x+\frac{1}{2}, -y+\frac{1}{2}, -z+2$	5.274	−5.2	−1.5	−12.6	6.7	−12.7	C7—O1···F2—C8	3.1436 (1), 100, 96
								C7—O1···F1—C8	3.0457, 139, 90
IV	$x, y, z+1$	8.360	−6.4	−1.6	−6.8	4.8	−10.0	C4—H4···O1	2.75, 134
								C5—H5···F2	2.63, 154
V	$x, -y, z+\frac{1}{2}$	8.524	−1.3	−2.3	−10.0	6.8	−6.9	H3···H2	2.40
								C3—H3···O1	2.95, 165
VI	$x, -y+1, z+\frac{1}{2}$	6.652	−0.7	−0.8	−8.2	3.7	−6.0	C6—H6···F2	2.69, 163
								C6—H6···F3	2.94, 124
								C8—F1···F2—C8	3.1023, 114, 147

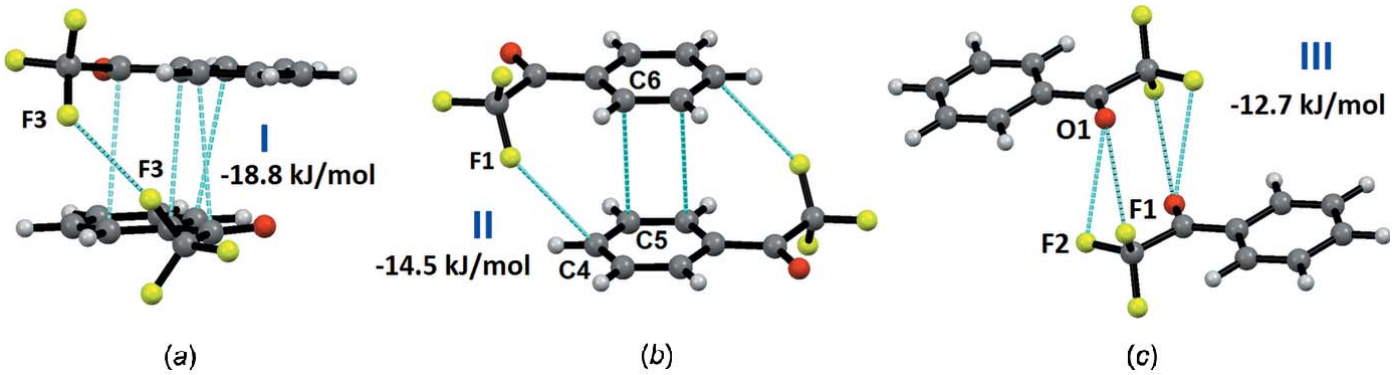

Figure 2
Molecular pairs (*a*) I, (*b*) II, and (*c*) III with their stabilization energies.

stabilized by the presence of π–π stacking and of different types of atom–atom contacts, such as intermolecular F···F, F···O, and H···H contacts.

The strongest molecular pair I (Fig. 2*a*), with an interaction energy of -18.8 kJ mol^{-1}, is formed *via* molecular stacking interactions and intermolecular type I F···F contacts [F3···F3, 2.8743 (1) Å and C8—F3···F3 139°]. In this case, the dispersion contribution (78%) is more significant in comparison to the electrostatic contribution towards the total stabilization of the dimer. The centrosymmetric molecular pair II (Fig. 2*b*), which is also formed due to π–π stacking, and to intermolecular F1···C4 interactions, shows an interaction energy of -14.5 kJ mol^{-1} (18% electrostatic and 82% dispersion contribution). Motif III (involving O1 with F1 and F2), with an interaction energy of -12.7 kJ mol^{-1}, is stabilized *via* intermolecular bifurcated F···O interactions with individual distances of 3.1436 (1) and 3.0457 Å (Fig. 2*c*). This shows how intermolecular F···O contacts provide a significant contribution towards the stabilization of the crystal packing, as already investigated in our recent study in terms of the associated nature and energetics (Sirohiwal *et al.*, 2017*b*).

The overall molecular arrangement shows the formation of a molecular sheet parallel to the *bc* plane (Fig. 3*a*). This sheet is constructed *via* the molecular pairs IV (-10.0 kJ mol^{-1}), V (-6.9 KJ mol^{-1}) and VI (-6.0 kJ mol^{-1}). It is interesting to note the dominance of the electrostatic (54%) over the dispersion (46%) contribution in case of motif IV, which is not to be found in other motifs. A molecular dimeric chain, associated with motif IV, is formed along the crystallographic *c*-axis direction, involving intermolecular C4—H4···O1 and C5—H5···F2 interactions (Table 1). Such dimeric chains are interlinked alternatively along the *b*-axis direction either *via* molecular pairs V (involving C4—H4···O1 interactions and H···H contacts) or VI (involving bifurcated C—H···F interactions and F···F contacts) related by *c*-glide symmetry. Finally, these parallel molecular sheets are stacked along the *a*-axis direction (Fig. 3*b*) *via* the strongest molecular pairs I. Thus, in the absence of any strong hydrogen bonds, the overall

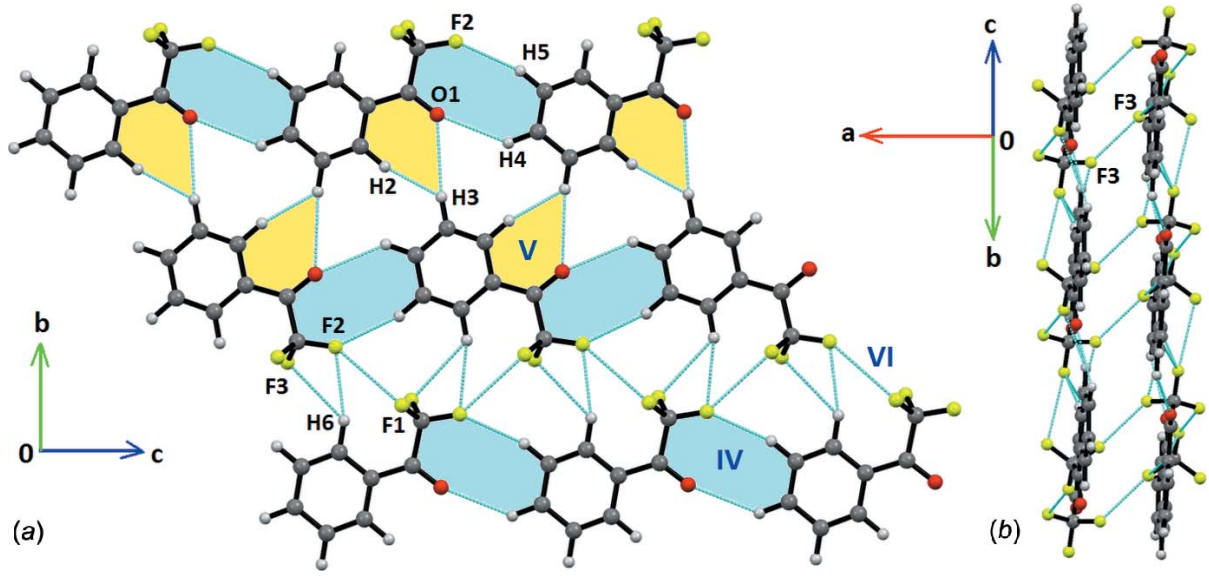

Figure 3
Packing network of TFAP showing (*a*) the molecular sheet formed *via* weak interactions in the *bc* plane and (*b*) the molecular stacking of two parallel sheets. Weak interactions are shown as cyan dotted lines.

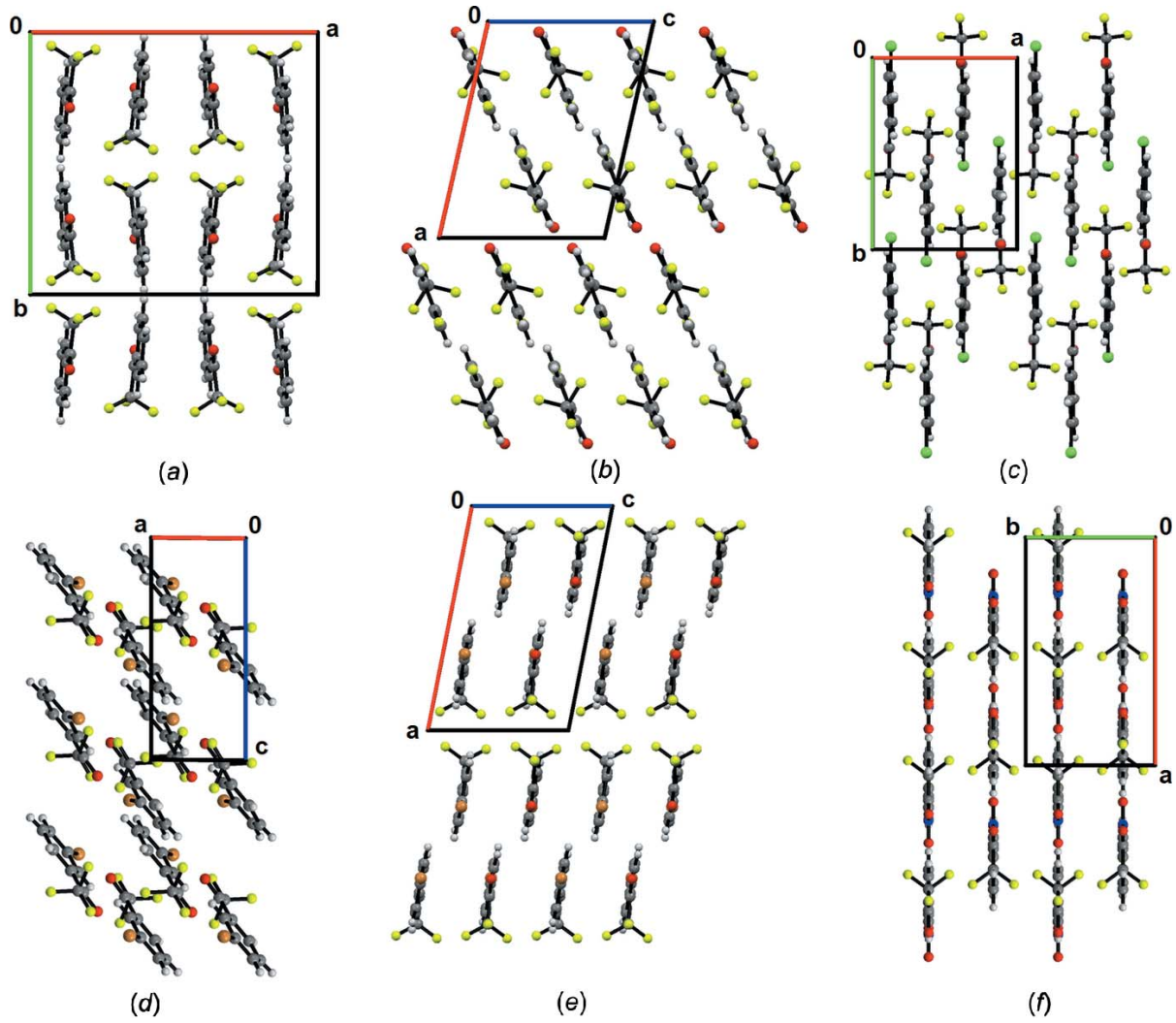

Figure 4
Molecular assembly in (*a*) TFAP and substituted TFAPs: (*b*) 4-fluoro TFAP, (*c*) 4-chloro TFAP, (*d*) 4-bromo TFAP, (*e*) 3-bromo TFAP and (*f*) 3-nitro TFAP.

crystal packing is stabilized through weak intermolecular interactions.

4. Database survey

Most of the substituted TFAPs are also liquid at room temperature and were crystallized *via in situ* cryocrystallization methods in the absence of OHCD. In particular, the crystal and molecular structures of 4-fluoro TFAP (SIDMAU), 4-chloro TFAP (SIDLUN), 4-bromo TFAP (SIDLOH), 3-bromo TFAP (SIDLEX), and 3-nitro TFAP (SIDLIB) have been obtained and reported (Chopra *et al.*, 2007).

Fig. 4 highlights the similarities and differences of the molecular assemblies for these structures in comparison to unsubstituted TFAP. Interestingly, in most of the cases, the molecular sheets are stacked on each other. The supramolecular assemblies are mainly stabilized *via* various weak C—H···O/F/Cl/Br/N interactions and F···F, F···O, Br···O, Br···F contacts without the presence of any strong interactions. Upon substitution with F, Cl, Br and $-NO_2$ groups, a molecular chain associated with F···F contacts is observed. In particular, in the case of the *para*-substituted chloro and bromo analogs, the F···F chain is quite similar, wherein in the case of the *para*-substituted fluoro compound, bifurcated F···F contacts are present. Finally, in the case of the *m*-nitro and bromo derivatives, a centrosymmetric, dimeric F···F chain is observed.

5. Hirshfeld surface analysis

The Hirshfeld surface analysis was performed using *CrystalExplorer3.3* (Turner *et al.*, 2017) to obtain two-dimensional fingerprint maps (Spackman *et al.*, 2002; McKinnon *et al.*, 2007), which help us to understand the crystalline environment in terms of the contributions of various interatomic contacts present in the crystal packing. The 2D fingerprint plots and the decomposed contributions for different atom–

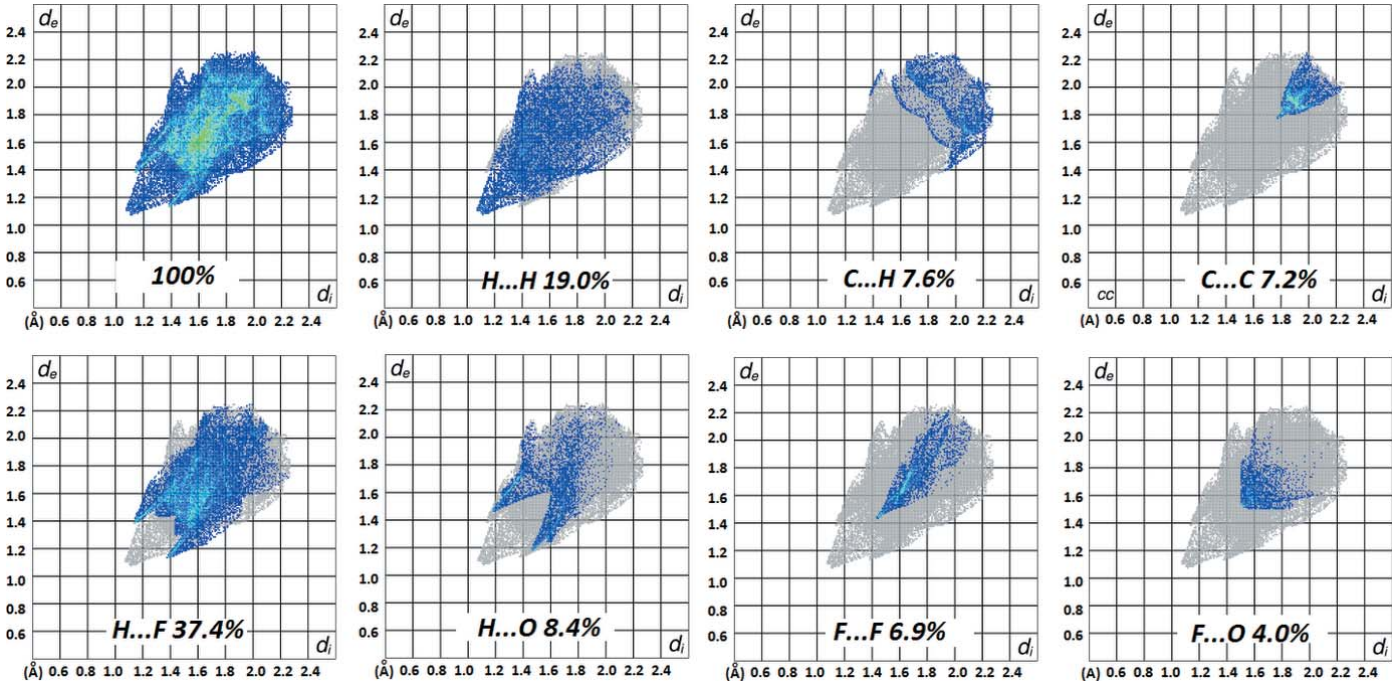

Figure 5
Two-dimensional fingerprint plots for TFAP, decomposed into contributions from specific atom–atom contacts.

atom contacts in unsubstituted TFAP are shown in Fig. 5. It is observed that the contributions for H···F (37.4%) and H···H (19.0%) contacts is relatively high in comparison to the other interatomic contacts. Interestingly, in this case, the fluorine atoms present in the $-CF_3$ group are more involved in the formation of C—H···F interactions rather than the formation of F··F (6.9%) contacts. The other contacts, namely C···H (7.6%), H···O (8.4%) and F···O (4.0%) also contribute to the overall crystal packing.

6. Crystallization, data collection and structure refinement

The compound TFAP was purchased from Sigma–Aldrich and used for the *in situ* crystallization experiment without any further purification. The detailed procedure of the crystallization process is already discussed in one of our previous reports (Dey *et al.*, 2016*a*). Good quality crystals (Fig. 6*a*) were obtained at 200 K using a CO_2 laser scan utilizing an OHCD apparatus. Fig. 6*b* and *c* depict the crystal at 110 (2) K inside the Lindemann glass capillary and the corresponding diffraction image, respectively. The crystal data, data collection and details on structure refinement are summarized in Table 3. All non-hydrogen atoms were refined anisotropically and the aromatic hydrogen atoms bonded to C atoms were positioned geometrically and refined using a riding model with $U_{iso}(H) = 1.2U_{eq}(C)$ and C—H distances of 0.95 Å.

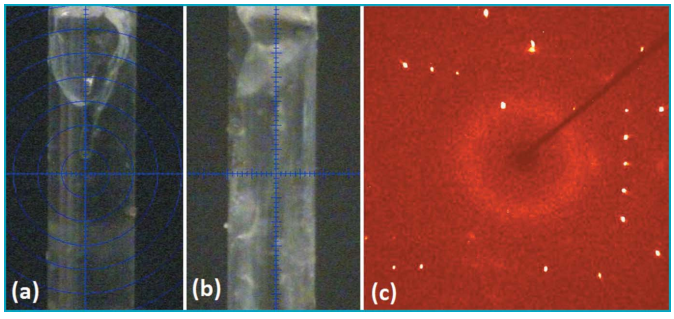

Figure 6
Crystal images at (*a*) 200 K, (*b*) 110 K, and (*c*) the diffraction image at 110 K.

Acknowledgements

DD acknowledges an Institute fellowship. AS would like to thank DST–INSPIRE Scholarship. DC would like to thank IISER Bhopal for the instrumental facility and infrastructure and DST–SERB for research funding.

References

Allen, F. H. (1986). *Acta Cryst.* B**42**, 515–522.
Altomare, A., Cascarano, G., Giacovazzo, C., Guagliardi, A., Burla, M. C., Polidori, G. & Camalli, M. (1994). *J. Appl. Cryst.* **27**, 435.
Boese, R., Kirchner, M. T., Billups, W. E. & Norman, L. R. (2003). *Angew. Chem. Int. Ed.* **42**, 1961–1963.
Bruker (2012). *APEX2*, *SAINT* and *SADABS*. Bruker AXS Inc., Madison, Wisconsin, USA.
Cakl, Z., Reimann, S., Schmidt, E., Moreno, A., Mallat, T. & Baiker, A. (2011). *J. Catal.* **280**, 104–115.
Chopra, D., Thiruvenkatam, V., Manjunath, S. G. & Guru Row, T. N. (2007). *Cryst. Growth Des.* **7**, 868–874.

Table 3
Experimental details.

Crystal data	
Chemical formula	$C_8H_5F_3O$
M_r	174.12
Crystal system, space group	Monoclinic, *C*2/*c*
Temperature (K)	110
a, *b*, *c* (Å)	13.8129 (3), 12.6034 (2), 8.3595 (2)
β (°)	90.396 (1)
V (Å^3)	1455.27 (5)
Z	8
Radiation type	Mo *K*α
μ (mm^{-1})	0.16
Crystal size (mm)	0.30 × 0.30 × 0.30
Data collection	
Diffractometer	Bruker APEXII CCD
Absorption correction	Multi-scan (*SADABS*; Bruker, 2012)
T_{min}, T_{max}	0.697, 0.746
No. of measured, independent and observed [$I > 2\sigma(I)$] reflections	9958, 1045, 944
R_{int}	0.014
$(\sin \theta/\lambda)_{max}$ (Å^{-1})	0.631
Refinement	
$R[F^2 > 2\sigma(F^2)]$, $wR(F^2)$, *S*	0.024, 0.064, 1.08
No. of reflections	1045
No. of parameters	109
H-atom treatment	H-atom parameters constrained
$\Delta\rho_{max}$, $\Delta\rho_{min}$ (e Å^{-3})	0.19, −0.20

Computer programs: *APEX2* and *SAINT* (Bruker, 2012), *SIR92* (Altomare *et al.*, 1994), *SHELXL2016/6* (Sheldrick, 2015), *Mercury* (Macrae *et al.*, 2008), *CIFTAB* (Sheldrick, 2008) and *PLATON* (Spek, 2009).

Choudhury, A. R., Winterton, N., Steiner, A., Cooper, A. I. & Johnson, K. A. (2005). *J. Am. Chem. Soc.* **127**, 16792–16793.

Dey, D., Bhandary, S., Sirohiwal, A., Hathwar, V. R. & Chopra, D. (2016*a*). *Chem. Commun.* **52**, 7225–7228.

Dey, D., Bhandary, S., Thomas, S. P., Spackman, M. A. & Chopra, D. (2016*b*). *Phys. Chem. Chem. Phys.* **18**, 31811–31820.

Frisch, M. J., *et al.* (2009). *GAUSSIAN*09, Revision D. 01. Gaussian Inc., Wallingford, CT, USA.

Gavezzotti, A. (2003). *J. Phys. Chem. B*, **107**, 2344–2353.

Gavezzotti, A. (2011). *New J. Chem.* **35**, 1360–1368.

Goubert, G., Demers-Carpentier, V., Masini, F., Dong, Y., Lemay, J. C. & McBreen, P. H. (2011). *Chem. Commun.* **47**, 9113–9115.

Guzmán-Gutiérrez, M. T., Zolotukhin, M. G., Fritsch, D., Ruiz-Treviño, F. A., Cedillo, G., Fregoso-Israel, E., Ortiz-Estrada, C., Chavez, J. & Kudla, C. (2008). *J. Membr. Sci.* **323**, 379–385.

Limnios, D. & Kokotos, C. G. (2014*a*). *J. Org. Chem.* **79**, 4270–4276.

Limnios, D. & Kokotos, C. G. (2014*b*). *Chem. Eur. J.* **20**, 559–563.

Macrae, C. F., Bruno, I. J., Chisholm, J. A., Edgington, P. R., McCabe, P., Pidcock, E., Rodriguez-Monge, L., Taylor, R., van de Streek, J. & Wood, P. A. (2008). *J. Appl. Cryst.* **41**, 466–470.

McKinnon, J. J., Jayatilaka, D. & Spackman, M. A. (2007). *Chem. Commun.* 3814-3816.

Sheldrick, G. M. (2008). *Acta Cryst.* A**64**, 112–122.

Sheldrick, G. M. (2015). *Acta Cryst.* C**71**, 3–8.

Sirohiwal, A., Hathwar, V. R., Dey, D. & Chopra, D. (2017*a*). *ChemPhysChem*, **18**, 2859–2863.

Sirohiwal, A., Hathwar, V. R., Dey, D., Regunathan, R. & Chopra, D. (2017*b*). *Acta Cryst.* B**73**, 140–152.

Spackman, M. A. & McKinnon, J. J. (2002). *CrystEngComm*, **4**, 378–392.

Spek, A. L. (2009). *Acta Cryst.* D**65**, 148–155.

Theodorou, A. & Kokotos, C. G. (2017*a*). *Green Chem.* **19**, 670–674.

Theodorou, A. & Kokotos, C. G. (2017*b*). *Adv. Synth. Catal.* **359**, 1577–1581.

Triandafillidi, I. & Kokotos, C. G. (2017). *Org. Lett.* **19**, 106–109.

Turner, M. J., McKinnon, J. J., Wolff, S. K., Grimwood, D. J., Spackman, P. R., Jayatilaka, D. & Spackman, M. A. (2017). *CrystalExplorer17*, University of Western Australia.http://hirshfeldsurface.net

supporting information

Acta Cryst. (2018). E**74**, 607-612 [https://doi.org/10.1107/S2056989017016590]

Crystal packing analysis of *in situ* cryocrystallized 2,2,2-trifluoroacetophenone

Dhananjay Dey, Abhishek Sirohiwal and Deepak Chopra

Computing details

Data collection: *APEX2* (Bruker, 2012); cell refinement: *SAINT* (Bruker, 2012); data reduction: *SAINT* (Bruker, 2012); program(s) used to solve structure: *SIR92* (Altomare *et al.*, 1994); program(s) used to refine structure: *SHELXL2016/6* (Sheldrick, 2015); molecular graphics: *Mercury* (Macrae *et al.*, 2008); software used to prepare material for publication: *CIFTAB* (Sheldrick, 2008) and *PLATON* (Spek, 2009).

2,2,2-Trifluoroacetophenone

Crystal data

$C_8H_5F_3O$
M_r = 174.12
Monoclinic, $C2/c$
a = 13.8129 (3) Å
b = 12.6034 (2) Å
c = 8.3595 (2) Å
β = 90.396 (1)°
V = 1455.27 (5) Å^3
Z = 8
$F(000)$ = 704
D_x = 1.589 Mg m^{-3}
Mo $K\alpha$ radiation, λ = 0.71073 Å
Cell parameters from 5549 reflections
θ = 2.2–30.2°
μ = 0.16 mm^{-1}
T = 110 K
Block, colorless
0.30 × 0.30 × 0.30 mm

Data collection

Bruker APEXII CCD diffractometer
Radiation source: fine focus sealed tube
ω scans
Absorption correction: multi-scan (SADABS; Bruker, 2008)
T_{min} = 0.697, T_{max} = 0.746
9958 measured reflections
1045 independent reflections
944 reflections with $I > 2\sigma(I)$
R_{int} = 0.014
θ_{max} = 26.7°, θ_{min} = 2.2°
$h = -17 \rightarrow 17$
$k = -15 \rightarrow 15$
$l = -5 \rightarrow 5$

Refinement

Refinement on F^2
Least-squares matrix: full
$R[F^2 > 2\sigma(F^2)]$ = 0.024
$wR(F^2)$ = 0.064
S = 1.08
1045 reflections
109 parameters
0 restraints
Hydrogen site location: inferred from neighbouring sites
H-atom parameters constrained
$w = 1/[\sigma^2(F_o^2) + (0.0305P)^2 + 0.8314P]$ where $P = (F_o^2 + 2F_c^2)/3$
$(\Delta/\sigma)_{max} < 0.001$
$\Delta\rho_{max}$ = 0.19 e Å^{-3}
$\Delta\rho_{min}$ = −0.20 e Å^{-3}

Special details

Geometry. All esds (except the esd in the dihedral angle between two l.s. planes) are estimated using the full covariance matrix. The cell esds are taken into account individually in the estimation of esds in distances, angles and torsion angles; correlations between esds in cell parameters are only used when they are defined by crystal symmetry. An approximate (isotropic) treatment of cell esds is used for estimating esds involving l.s. planes.

Fractional atomic coordinates and isotropic or equivalent isotropic displacement parameters (Å²)

	x	*y*	*z*	U_{iso}*/U_{eq}
F1	0.27357 (5)	0.43371 (5)	0.83259 (12)	0.0310 (3)
F2	0.33321 (6)	0.40770 (6)	1.06711 (16)	0.0376 (4)
F3	0.42716 (5)	0.44771 (5)	0.87193 (13)	0.0331 (3)
O1	0.36355 (6)	0.21263 (7)	0.98806 (15)	0.0268 (3)
C4	0.39488 (8)	0.16370 (10)	0.3960 (2)	0.0278 (5)
H4	0.402903	0.138083	0.290060	0.033*
C5	0.38764 (9)	0.27193 (10)	0.4248 (2)	0.0273 (5)
H5	0.390579	0.320406	0.337898	0.033*
C6	0.37625 (8)	0.30955 (9)	0.5781 (2)	0.0223 (5)
H6	0.371252	0.383735	0.596420	0.027*
C1	0.37202 (7)	0.23921 (9)	0.7068 (2)	0.0176 (5)
C7	0.36188 (7)	0.27209 (9)	0.8742 (2)	0.0200 (5)
C8	0.34856 (9)	0.39204 (9)	0.9128 (3)	0.0241 (5)
C3	0.39028 (9)	0.09306 (9)	0.5237 (2)	0.0259 (5)
H3	0.395028	0.018927	0.504787	0.031*
C2	0.37893 (8)	0.12990 (9)	0.6766 (2)	0.0235 (5)
H2	0.375707	0.081052	0.762999	0.028*

Atomic displacement parameters (Å²)

	U^{11}	U^{22}	U^{33}	U^{12}	U^{13}	U^{23}
F1	0.0323 (4)	0.0267 (4)	0.0339 (10)	0.0079 (3)	0.0017 (4)	0.0015 (3)
F2	0.0604 (5)	0.0314 (4)	0.0210 (13)	0.0015 (3)	0.0051 (5)	−0.0069 (4)
F3	0.0336 (4)	0.0239 (3)	0.0420 (9)	−0.0065 (3)	0.0030 (4)	−0.0046 (3)
O1	0.0382 (5)	0.0281 (4)	0.0142 (12)	−0.0003 (3)	0.0004 (4)	0.0047 (5)
C4	0.0263 (6)	0.0403 (7)	0.0169 (16)	−0.0026 (5)	0.0001 (6)	−0.0063 (7)
C5	0.0330 (6)	0.0347 (7)	0.0141 (19)	−0.0028 (5)	0.0007 (6)	0.0079 (7)
C6	0.0281 (6)	0.0234 (6)	0.0156 (18)	−0.0001 (4)	0.0004 (6)	0.0031 (6)
C1	0.0193 (5)	0.0217 (5)	0.0118 (17)	−0.0007 (4)	−0.0007 (5)	0.0013 (6)
C7	0.0207 (5)	0.0220 (6)	0.0171 (17)	−0.0011 (4)	−0.0002 (5)	0.0032 (7)
C8	0.0296 (6)	0.0248 (6)	0.018 (2)	−0.0003 (4)	0.0021 (6)	−0.0021 (6)
C3	0.0338 (6)	0.0253 (6)	0.0187 (17)	−0.0013 (4)	0.0001 (6)	−0.0048 (7)
C2	0.0293 (6)	0.0215 (6)	0.0197 (18)	−0.0011 (4)	−0.0012 (6)	0.0026 (6)

Geometric parameters (Å, º)

F1—C8	1.3373 (17)	C6—C1	1.396 (2)
F2—C8	1.324 (2)	C6—H6	0.9500
F3—C8	1.3389 (15)	C1—C2	1.4040 (15)

O1—C7	1.2112 (18)	C1—C7	1.467 (2)
C4—C5	1.3888 (19)	C7—C8	1.5569 (16)
C4—C3	1.392 (2)	C3—C2	1.370 (2)
C4—H4	0.9500	C3—H3	0.9500
C5—C6	1.377 (2)	C2—H2	0.9500
C5—H5	0.9500		

C5—C4—C3	119.46 (17)	C1—C7—C8	118.93 (13)
C5—C4—H4	120.3	F2—C8—F1	107.54 (12)
C3—C4—H4	120.3	F2—C8—F3	107.82 (12)
C6—C5—C4	120.53 (15)	F1—C8—F3	107.05 (12)
C6—C5—H5	119.7	F2—C8—C7	111.48 (12)
C4—C5—H5	119.7	F1—C8—C7	111.71 (12)
C5—C6—C1	120.32 (13)	F3—C8—C7	111.03 (11)
C5—C6—H6	119.8	C2—C3—C4	120.33 (13)
C1—C6—H6	119.8	C2—C3—H3	119.8
C6—C1—C2	118.78 (16)	C4—C3—H3	119.8
C6—C1—C7	124.10 (12)	C3—C2—C1	120.58 (14)
C2—C1—C7	117.11 (13)	C3—C2—H2	119.7
O1—C7—C1	124.96 (12)	C1—C2—H2	119.7
O1—C7—C8	116.10 (16)		

C3—C4—C5—C6	0.17 (18)	C1—C7—C8—F2	175.26 (9)
C4—C5—C6—C1	0.12 (17)	O1—C7—C8—F1	−125.49 (14)
C5—C6—C1—C2	−0.42 (16)	C1—C7—C8—F1	54.91 (16)
C5—C6—C1—C7	178.79 (10)	O1—C7—C8—F3	115.10 (15)
C6—C1—C7—O1	−175.62 (11)	C1—C7—C8—F3	−64.50 (17)
C2—C1—C7—O1	3.60 (16)	C5—C4—C3—C2	−0.15 (18)
C6—C1—C7—C8	3.94 (15)	C4—C3—C2—C1	−0.15 (17)
C2—C1—C7—C8	−176.84 (10)	C6—C1—C2—C3	0.43 (16)
O1—C7—C8—F2	−5.15 (14)	C7—C1—C2—C3	−178.83 (10)

Hydrogen-bond geometry (Å, º)

D—H···*A*	*D*—H	H···*A*	*D*···*A*	*D*—H···*A*
C6—H6···F1	0.95	2.48	3.004 (2)	115
C6—H6···F3	0.95	2.55	3.088 (2)	116
C5—H5···F2^{i}	0.95	2.63	3.522 (2)	156
C4—H4···O1^{i}	0.95	2.74	3.490 (2)	136
C6—H6···F2^{ii}	0.95	2.69	3.614 (2)	163
C6—H6···F3^{ii}	0.95	2.94	3.584 (2)	126
C5—H5···F3^{ii}	0.95	2.98	3.603 (2)	124
C3—H3···O1^{iii}	0.95	2.95	3.882 (2)	166

Symmetry codes: (i) *x*, *y*, *z*−1; (ii) *x*, −*y*+1, *z*−1/2; (iii) *x*, −*y*, *z*−1/2.